

Spectroscopic investigations of new binuclear transition metal complexes of Schiff bases derived from 4,6-diacetylresorcinol and 3-amino-1-propanol or 1,3-diamino-propane

Adel A.A. Emara*, Akila A. Saleh, Omima M.I. Adly

Department of Chemistry, Faculty of Education, Ain Shams University, Roxy, Cairo 11341, Egypt

Received 25 November 2006; accepted 17 December 2006

Abstract

The bifunctional carbonyl compound; 4,6-diacetylresorcinol (DAR) serves as precursor for the formation of different Schiff base ligands, which are either di- or tetra-basic with two symmetrical sets of either O₂N or N₂O tridentate chelating sites. The condensation of 4,6-diacetylresorcinol with 3-amino-1-propanol (3-AP) or 1,3-diaminopropane (DAP), yields the corresponding hexadentate Schiff base ligands, abbreviated as H₄L_a and H₂L_b, respectively. The structures of these ligands were elucidated by elemental analyses, IR, mass, ¹H NMR and electronic spectra. Reaction of the Schiff base ligands with copper(II), nickel(II), cobalt(II), zinc(II), cadmium(II), iron(III), chromium(III), vanadyl(IV) and uranyl(VI) ions in 1:2 molar ratio afforded the corresponding transition metal complexes. A variety of binuclear complexes for the metal complexes were obtained with the ligands in its di- or tetra-deprotonated forms. The structures of the newly prepared complexes were identified by elemental analyses, infrared, electronic, mass, ¹H NMR and ESR spectra as well as magnetic susceptibility measurements and thermal gravimetric analysis (TGA). The bonding sites are the azomethine and amino nitrogen atoms, and phenolic and alcoholic oxygen atoms. The metal complexes exhibit different geometrical arrangements such as square planar, tetrahedral, square pyramid and octahedral arrangement.
© 2007 Elsevier B.V. All rights reserved.

Keywords: Schiff base ligands; Binuclear complexes; 4,6-Diacetylresorcinol; 3-Amino-1-propanol and 1,3-diaminopropane

1. Introduction

A large number of Schiff bases and their metal complexes have been studied because of their interesting and important properties such as their ability to reversibly bind oxygen [1], and their use in catalyses for: oxygenation and oxidation reactions of organic compounds [2], redox systems in biological processes [3], Aldol reactions [4], degradation of dyes through decomposition of hydrogen peroxide and other reagents, in textile industries [5], reduction of thionyl chloride [6] and oxidation of DNA [7]. Also Schiff bases can be used in degradation of organic compounds [8] and in radiopharmaceuticals [9]. For these applications, we are extending this field in synthesis of novel binuclear Schiff base complexes.

The present study, is extension to our work [10,11] where the ligands were prepared by the condensation of

4,6-diacetylresorcinol, as starting material, with 3-amino-1-propanol (3-AP) and 1,3-diaminopropane (DAP) to afford the corresponding Schiff base, H₄L_a and H₂L_b ligands, respectively. The reactions of these ligands with some transition metal ions in molar ratio (1:2, ligand:metal ion) were studied. The newly prepared metal complexes of these ligands were identified by different physicochemical and spectroscopic techniques.

The Schiff base, H₄L_a and H₂L_b ligands were allowed to react with copper(II), nickel(II), cobalt(II), cadmium(II), zinc(II), iron(III), chromium(III), vanadyl(IV) and uranyl(VI) ions. All reactions afforded binuclear complexes except cadmium(II) and zinc(II) for H₄L_a ligand, and zinc(II) and iron(III) for H₂L_b ligand, which gave oily products which were difficult to isolate. For the former ligand, the copper(II) complex exhibits a square planar geometry, while nickel(II), cobalt(II) and iron(III) complexes exhibit an octahedral geometry which contain nitrate ions acting as unidentate ligands, also, the chromium(III) complex showed an octahedral geometry but the nitrate ions acting as bidentate ligand. The vanadyl(IV) complex showed a square pyramidal geometry and the uranyl(VI) complex has a coordination number = 8. The bonding sites are the azomethine nitrogen atoms and

* Corresponding author. Tel.: +20 2 4551530; fax: +20 2 4530271.

E-mail addresses: adelaemara@yahoo.com,
adelaemara@gmail.com (A.A.A. Emara).

the phenolic and alcoholic oxygen atoms. For the H_2L_b ligand, all complexes having octahedral environment around Cu(II), Ni(II), Co(II), Fe(III) Cr(III), VO(IV) and UO₂(VI) ions. The bonding sites are the azomethine and amino nitrogen atoms and the phenolic oxygen atoms, except uranyl(VI) complex, where the amino nitrogen atoms are not involved in the coordination. Most of the complexes of the H_2L_b ligand contain nitrate ions which acting as unidentate ligands, also, in case of vanadyl(IV) complex, the SO_4^{2-} ions is involved in the coordination and acts as a bridged ligand.

2. Experimental

2.1. Materials

Resorcinol, acetic anhydride, zinc chloride, 3-amino-1-propanol and 1,3-diaminopropane were either Analar or Merck. Copper(II), nickel(II), cobalt(II), cadmium(II), zinc(II), iron(III) and chromium(III) were used as nitrate salts and were Merck or BDH. Uranyl(VI) acetate dihydrate and vanadyl(IV) sulphate monohydrate were Merck or BDH. Organic solvents (ethanol, absolute ethanol, methanol, diethylether, acetone, dimethylformamide (DMF) and dimethylsulfoxide (DMSO)) were reagent grade.

2.2. Synthesis of the Schiff base ligands

Schiff base ligands were prepared in two steps. The first step was the formation of 4,6-diacetylresorcinol (DAR) by acetylation of resorcinol. The second step was the condensation of 4,6-diacetylresorcinol (DAR) stoichiometrically in a molar ratio 1:2 with 3-amino-1-propanol or 1,3-diaminopropane in absolute ethanol. The Schiff base ligands were formed by stirring the reaction for 1 h at room temperature. If the ligand did not precipitate, the reaction was heated to reflux for 1–3 h, where the solid was formed.

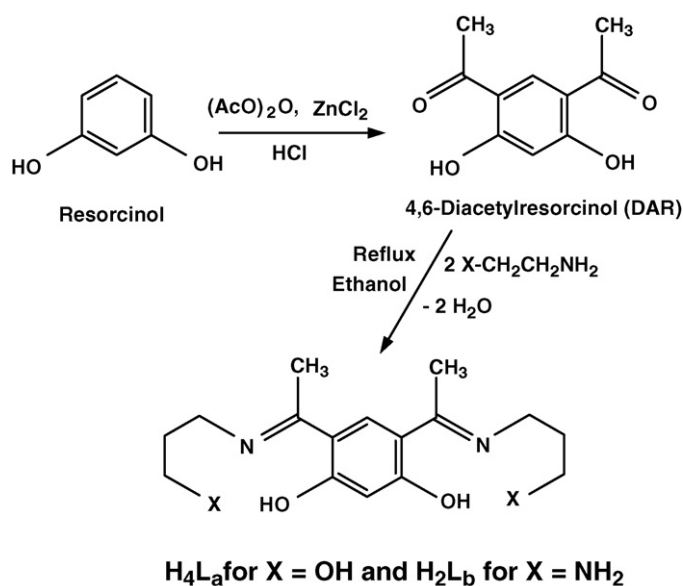
The Schiff base, H_4L_a and H_2L_b ligands were characterized by elemental analysis, ¹H NMR spectroscopy and UV–vis spectrophotometer in DMF or DMSO and in the solid state by FT-IR and mass spectroscopy. The synthetic steps are given in details as follows.

2.2.1. Synthesis of 4,6-diacetylresorcinol

The method of preparation was the same as mentioned in Ref. [10]. The yield was 10.0 g (28.4%), mp 178–180 °C. 4,6-Diacetylresorcinol was characterized by elemental analysis and infrared spectrum.

2.2.2. Synthesis of the Schiff base, H_4L_a and H_2L_b ligands

The H_4L_a and H_2L_b ligands were synthesized by adding 4,6-diacetylresorcinol, DAR (3.88 g, 20.0 mmol) dissolved in hot absolute ethanol (30 mL) to 3-amino-1-propanol (3.00 g, 40.0 mmol) or 1,3-diaminopropane (2.96 g, 40.0 mmol) in absolute ethanol (30 mL). The reaction mixtures were heated to reflux for 1–3 h. The yellow products obtained were filtered off and washed with few amounts of ethanol then diethylether and air dried. Fine crystals were obtained by recrystallization



Scheme 1. Schematic representation for the formation of the Schiff base, H_4L_a and H_2L_b ligands. Structure 1. Representative structures of the Schiff base, H_4L_a and H_2L_b ligands.

from ethanol. The ligands were kept in a desiccator until used. The yield was 5.00 g (81.0%), and 4.80 g (78.1%), for H_4L_a and H_2L_b , respectively. The melting point (mp) for both ligands were >280 °C.

The reaction for the formation of 4,6-diacetylresorcinol and their corresponding H_4L_a and H_2L_b ligands are illustrated in Scheme 1.

2.3. Synthesis of the Schiff base metal complexes

Methanolic solutions of the metal salts (30 mL) were added gradually to methanolic solutions of the deprotonated ligand (60 mL) in the molar ratio 2:1. Triethylamine, Et₃N, was used to affect the deprotonation of the ligands. The reaction mixture of the deprotonated H_4L_a ligand with metal salts was stirred on cold for 1–3 h, while the reaction mixture of the other ligand, H_2L_b , was heated to reflux for 2–3 h. The time of reflux depends on the formation of the solid products on either hot or cold. The resulting precipitates were filtered off, washed with methanol then ether. Most of the complexes are insoluble in most common organic solvents, but some of them are partially soluble in DMF and/or DMSO.

In each case, the ligand is deprotonated using Et₃N. In the case of H_4L_a ligand, Et₃N (1.212 g, 12 mmol) dissolved in methanol (20 mL) was added to 3 mmol of the ligand in 30 mL methanol, i.e., in the molar ratio 4:1 (Et₃N:ligand) and heated to reflux for 30 min. The appropriate weight (6 mmol) of the metal salts was added to the ionic deprotonated ligand to form the metal complexes. In the case of H_2L_b , the same procedure was used, however, the molar ratio was 2:1 (Et₃N:ligand).

The following detailed preparations are given as examples and the other complexes were obtained similarly.

2.3.1. Reaction of Cu(II) with H₄L_a to form complex (1)

Copper(II) nitrate tetrahydrate, Cu(NO₃)₂·4H₂O (1.45 g, 6 mmol) in methanol (30 mL) was added gradually with constant stirring to a solution of the deprotonated ligand, H₄L_a (0.918 g, 3 mmol) in methanol (60 mL). The stoichiometry of the metal ion to ligand was 2:1. The solution was stirred for 1 h. A green precipitate was formed and washed with small amount of methanol then ether. The yield was 0.96 g (51.6%), mp > 280 °C.

2.3.2. Reaction of VO(IV) with H₂L_b to form complex (13)

Vanadyl(IV) sulphate monohydrate, VOSO₄·H₂O (1.06 g, 6 mmol) in methanol (30 mL) and small amount of distilled water was added gradually with constant stirring to a solution of the deprotonated ligand (0.918 g, 3 mmol) in methanol (60 mL). The solution was heated to reflux for 3 h. A green precipitate was obtained and washed with small amount of methanol then ether. The yield was 0.95 g (52.8%), mp > 280 °C.

The effect of the triethylamine as deprotonating agent was investigated, and did not coordinate as a ligand with the metal ions.

2.3.3. Unsuccessful trials

Trials to prepare Cd(II) and Zn(II) complexes of the Schiff base, H₄L_a, ligand and Zn(II) and Fe(III) complexes of the Schiff base, H₂L_b, ligand were unsuccessful, which gave oily products which were not isolated in their pure forms.

2.4. Physical measurements

The analyses of carbon, hydrogen and nitrogen were carried out at the Microanalytical Center, Cairo University, Giza, Egypt. Analyses of metal ions after the dissolution of the solid complex in hot concentrated nitric acid, HNO₃, then diluting with distilled water and filtering to remove the precipitated ligand. The solution was neutralized with ammonia solution and the metal ions were then titrated with EDTA [12–14]. The FT-IR spectra (4000–400 cm⁻¹) of the compounds were recorded as KBr discs using FT-IR (Shimadzu) spectrophotometer model 4000. Absorption frequencies are given in wavenumbers (cm⁻¹). ¹H NMR spectra were recorded using a Varian spectrometer, EM-390, 90 MHz. Dimethyl-sulphoxide, DMSO-*d*₆, was used as a solvent and tetramethylsilane (TMS) as an internal reference. The spectra were extended from 0 to 18 ppm. The chemical shifts (δ) are given down field relative to TMS. D₂O was added to every sample to test for the deuteration of the samples. Reflectance spectra of the compounds were recorded as NaCl discs using a Shimadzu UV–vis spectrophotometer 1601 provided with a diffuse reflectance attachment. Reflectance was carried out at 5° incidence angle in the range 400–1200 nm. The solution spectra of the ligands were also carried out in 10⁻³ M of either DMF or DMSO solution on a JASCO model V-550 UV–vis spectrophotometer in the range 200–500 nm. Magnetic susceptibilities of the complexes were measured by the Gouy method at room temperature using Johnson Matthey, Alfa product, Model No. (MKI), Magnetic Susceptibility Balance. Effective magnetic moments were calculated from the expression $\mu_{\text{eff}} (\mu_{\text{B}}) = 2.828 (\chi_{\text{M}} \times T)^{1/2}$, where χ_{M} is the molar susceptibility [15]. Diamag-

netic corrections were calculated from Pascal's constants for all atoms in the compounds [15]. Thermal gravimetric analysis (TGA) data was measured from room temperature up to 800 °C at a heating rate of 20 °C/min. The data were obtained using a Shimadzu TGA-50H instrument. Melting points reported in this work were not corrected. ESR spectra of compounds were recorded on the Bruker, Model: EMX, X-band spectrometer. Mass spectra of the compounds were recorded on a Hewlett Packard mass spectrometer model MS 5988. Samples were introduced directly to the probe, and the fragmentations were carried out at 300 °C and 70 eV.

3. Results and discussion

3.1. The Schiff base, H₄L_a and H₂L_b ligands

The Schiff base, H₄L_a, and H₂L_b ligands were prepared by the condensation of 4,6-diacetylresorcinol (DAR) with 3-amino-1-propanol (3-AP) or 1,3-diaminopropane (DAP) in molar ratio 1:2. The structures are identified by elemental analyses, infrared, UV–vis, ¹H NMR and mass spectra. Table 1 lists the physical and analytical data of the Schiff base, H₄L_a, and H₂L_b ligands and their transition metal complexes. From the investigation, the H₄L_a, and H₂L_b ligands can be represented in Structure 1.

The infrared frequencies of the Schiff base, H₄L_a and H₂L_b ligands along with 4,6-diacetylresorcinol (DAR), 3-amino-1-propanol (3-AP) and 1,3-diaminopropane (DAP), and their assignments are listed in Table 2. The infrared spectra are consistent with the formation of H₄L_a and H₂L_b ligands. The vibrational assignments were aided by comparison with the vibrational frequencies of the related compounds, such as, the Schiff bases of salicylaldehyde [16]. The fundamental stretching mode of the azomethine moiety, $\nu(\text{C}=\text{N}-)$, is readily assigned by comparison with the infrared spectra of 4,6-diacetylresorcinol (DAR), 3-amino-1-propanol(3-AP) and 1,3-diaminopropane (DAP). This intense band at 1578 and 1575 cm⁻¹ for H₄L_a and H₂L_b ligands, respectively, are assigned to the $\text{C}=\text{N}$ stretching frequency of both ligands and are characterized for the azomethine moiety of most Schiff base compounds. The absorption band of the C=O in the 4,6-diacetylresorcinol disappeared in the infrared spectrum of the ligand, which indicate that the condensation has occurred. The $\nu(\text{NH}_2)$ stretching frequencies of DAP which lies at 3357 and 3283 cm⁻¹ still persist even after the formation of the H₂L_b ligand. This could be due to one of the two NH₂ groups of DAP is participating in the condensation with DAR, while the other NH₂ group still free in H₂L_b ligand and did not disappear in the infrared spectrum of H₂L_b. On the other hand, other fundamental bands were assigned in the infrared spectra of H₄L_a and H₂L_b ligands. Of these, the fundamental stretching bands which are the $\nu(\text{C}-\text{C})$ aliphatic, $\nu(\text{OH})$ aliphatic, $\nu(\text{OH})$ aromatic, $\nu(\text{CH}_3)$, $\nu(\text{C}-\text{C})$ aromatic, $\nu(\text{C}=\text{N}-)$, $\nu(\text{C}-\text{O})$, $\nu(\text{ArC}-\text{H})$, $\nu(\text{C}-\text{N})$, $\nu(\text{CH}_2)$ and the bending bands which are the $\delta(\text{H}-\text{OC})$ aliphatic, $\delta(\text{H}-\text{OC})$ aromatic, $\delta(\text{CCC})$ aliphatic, $\delta(\text{CH}_2)$ aliphatic, $\delta(\text{C}-\text{C}=\text{N})$, $\delta(\text{N}=\text{C}-\text{C})$, $\delta(\text{CH}_3)$, $\delta(\text{ArC}-\text{H})$, in plane, (ArC–H) out of plane, $\rho r(\text{CH}_3)$, $\rho r(\text{CH}_2)$, $\rho w(\text{CH}_3)$ and $\rho w(\text{CH}_2)$ are identified (Table 2).

Table 1
Physical and analytical data of the Schiff base, H₄L_a and H₂L_b ligands and their transition metal complexes

Ligand/complex	Molecular formula	M. wt. yield (%)	Color	mp (°C)	C	H	N	M
H ₄ L _a	C ₁₆ H ₂₄ N ₂ O ₄	308.4 (81.0)	Yellow	>280	62.50 (62.32)	7.94 (7.85)	8.99 (9.08)	–
H ₂ L _b	C ₁₆ H ₂₆ N ₄ O ₂	306.4 (78.1)	Yellow	>280	62.80 (62.70)	8.60 (8.60)	18.42 (18.39)	–
(1) [Cu ₂ (H ₂ L _a)(NO ₃) ₂]·2CH ₃ OH	C ₁₈ H ₃₀ N ₄ O ₁₂ Cu ₂	621.0 (75.6)	Green	>280	35.32 (34.78)	4.31 (4.87)	8.98 (9.01)	21.08 (20.45)
(2) [Ni ₂ (H ₂ L _a)(NO ₃) ₂ (CH ₃ OH) ₂ (H ₂ O) ₂]	C ₁₈ H ₃₄ N ₄ O ₁₄ Ni ₂	647.9 (46.4)	Green	>280	33.77 (33.37)	5.48 (5.29)	8.58 (8.65)	18.25 (18.12)
(3) [Co ₂ (H ₂ L _a)(H ₂ O) ₂ (CH ₃ OH) ₂ (NO ₃) ₂]	C ₁₈ H ₃₄ N ₄ O ₁₄ Co ₂	648.4 (57.2)	Green	>280	33.80 (33.35)	5.20 (5.29)	8.24 (8.64)	18.15 (18.18)
(4) [Fe ₂ (L _a)(H ₂ O) ₂ (NO ₃) ₂]·2H ₂ O	C ₁₆ H ₃₂ N ₄ O ₁₆ Fe ₂	648.1 (65.4)	Red	>280	29.95 (29.65)	4.44 (4.98)	7.97 (8.65)	17.30 (17.23)
(5) [Cr ₂ (L _a)(H ₂ O) ₂ (NO ₃) ₂]·2H ₂ O·3CH ₃ OH	C ₁₉ H ₄₂ N ₆ O ₂₃ Cr ₂	826.6 (76.5)	Dark green	>280	27.88 (27.61)	5.12 (5.12)	9.89 (10.17)	12.52 (12.58)
(6) [(VO) ₂ (L _a)(H ₂ O) ₂]·2H ₂ O	C ₁₆ H ₂₈ N ₂ O ₁₀ V ₂	509.9 (60.8)	Green	>280	38.00 (37.65)	5.21 (5.49)	5.77 (5.49)	–
(7) [(UO ₂) ₂ (H ₂ L _a) ₂]·6H ₂ O	C ₃₂ H ₅₆ N ₄ O ₁₈ U ₂	1260.0 (48.7)	Yellow	>280	30.45 (30.48)	4.60 (4.48)	4.01 (4.44)	–
(8) [Cu ₂ (L _b)(NO ₃) ₂ (H ₂ O) ₄]·H ₂ O	C ₁₆ H ₃₄ N ₆ O ₁₃ Cu ₂	645.6 (46.6)	Green	>280	29.80 (29.80)	5.30 (5.30)	13.21 (13.11)	19.67 (19.69)
(9) [Ni ₂ (L _b)(NO ₃) ₂ (H ₂ O) ₄]·2CH ₃ OH	C ₁₈ H ₄₀ N ₆ O ₁₄ Ni ₂	681.4 (70.2)	Cumin	>280	32.48 (31.73)	5.62 (5.81)	12.50 (12.33)	17.14 (17.23)
(10) [Co ₂ (L _b)(NO ₃) ₂ (H ₂ O) ₄]·3H ₂ O	C ₁₆ H ₃₈ N ₆ O ₁₅ Co ₂	672.4 (54.7)	Green	>280	28.68 (28.58)	5.80 (5.70)	12.42 (12.51)	17.60 (17.53)
(11) [Cd ₂ (L _b)(NO ₃) ₂ (H ₂ O) ₄]·3H ₂ O	C ₁₆ H ₃₈ N ₆ O ₁₅ Cd ₂	779.3 (34.3)	Yellow	>280	24.56 (24.66)	4.35 (4.92)	10.69 (10.80)	28.88 (28.85)
(12) [Cr ₂ (L _b)(NO ₃) ₂ (H ₂ O) ₂]·4.5H ₂ O	C ₁₆ H ₃₇ N ₈ O _{20.5} Cr ₂	773.5 (23.8)	Green	>280	24.80 (24.85)	5.20 (4.82)	14.43 (14.54)	13.39 (13.44)
(13) [(VO) ₂ (L _b)(SO ₄)(H ₂ O) ₂]·2H ₂ O	C ₁₆ H ₃₂ N ₄ O ₁₂ SV ₂	606.4 (66.3)	Green	>280	31.48 (31.69)	5.24 (5.32)	9.25 (9.20)	–
(14) [(UO ₂) ₂ (L _b) ₂ (H ₂ O) ₄]·4H ₂ O	C ₃₂ H ₆₄ N ₈ O ₁₆ U ₂	1292.9 (40.6)	Yellow	>280	29.90 (29.73)	5.00 (4.99)	8.83 (8.79)	–

The mass spectra of the Schiff base, H₄L_a and H₂L_b ligands, revealed the molecular ion peaks at *m/e* 308 and 306, respectively, which are coincident with the formula weights (308.4 and 306.4) for H₄L_a and H₂L_b ligands and supports the identity of the structures. The fragmentation patterns of the mass spectrum of the H₄L_a ligand is depicted in Scheme 2.

¹H NMR spectra of H₄L_a and H₂L_b ligands in deuterated dimethyl-sulphoxide, DMSO-*d*₆, without and with D₂O are shown in Fig. 1. The chemical shifts of the proton signals in the spectrum of the Schiff base, H₄L_a and H₂L_b ligands with their assignments are listed in Table 3. The proton signals of the –OH for the alcoholic (4.62 ppm) and phenolic (17.28 ppm) protons in the former ligand and the proton signals of the –NH₂ group at 3.31 ppm and –OH group at 17.28 ppm, in the later ligand disappeared in the presence of D₂O, which indicate that these protons are acidic and the hydroxyl groups can participate in the coordination with the metal ions. The ¹H NMR spectra of the both ligands in DMSO-*d*₆ showed different tautomeric species for the same ligands. The proposed tautomeric forms I–IV is illustrated in Scheme 3. It is expected that the tautomeric form I is more favorable and the tautomeric form IV is less favorable. On the other hand, it is clear that the tautomeric forms II and III are in a similar chemical environment and expected to show the same signals. The aromatic proton signals, which are centered at 5.86 and 8.17 ppm, in the H₄L_a spectra, and at 5.65 and 8.00 ppm for the H₂L_b spectra, can be used as a probe to detect the ratio of these tautomeric forms. The integrated ratio of I:(II and III):IV tautomeric forms are 56:40:4 for the H₄L_a ligand and 50:48:2 for the H₂L_b ligand, in DMSO-*d*₆ solvent.

Electronic spectral data of the H₄L_a and H₂L_b ligands were recorded in DMF solution. In the electronic spectra of the ligands, four absorption bands at 220, 315, 365 and 390 nm for the former ligand and 265, 278, 339 and 371 nm for the later ligand were characterized. In both cases, the first two bands correspond to ¹L_a → ¹A₁ and ¹L_b → ¹A₁ transitions of the phenyl ring [17]. The third band corresponds to the π → π* transition of the azomethine group, and the last band corresponds to the n → π* transition which is overlapped with the intermolecular CT from the phenyl ring [18,19].

3.2. Schiff base complexes of H₄L_a and H₂L_b ligands

Although, the Schiff base, H₄L_a, ligand behaves as a di- or tetra-basic ligand with two O₂N tridentate sites, the Schiff base, H₂L_b, ligand behaves as dibasic ligand with two N₂O tridentate sites. The two ligands reacted with Cu(II), Ni(II), Co(II), Cd(II), Cr(III), Fe(III), VO(IV) and UO₂(VI) ions to yield the corresponding binuclear transition metal complexes. The isolated transition metal complexes were identified by different techniques such as elemental analyses, FT-IR, ¹H NMR, mass, UV–vis, ESR spectroscopy and thermal gravimetric analysis (TGA), beside, the magnetic susceptibility measurements.

3.2.1. Infrared spectra

IR spectra of the complexes were recorded to confirm their structures. The vibrational frequencies and their tentative assignments for the H₄L_a and H₂L_b ligands and their transition metal

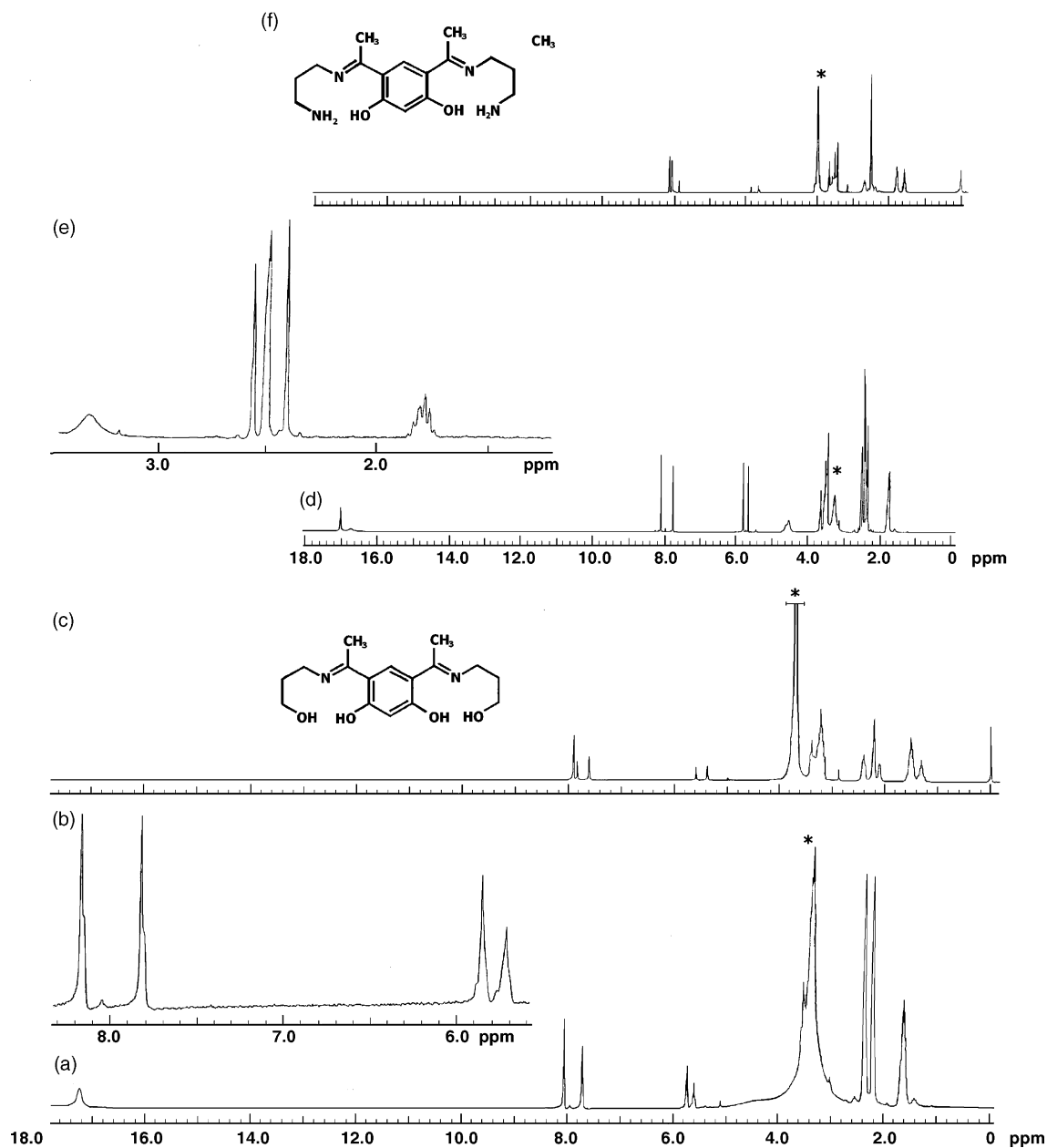


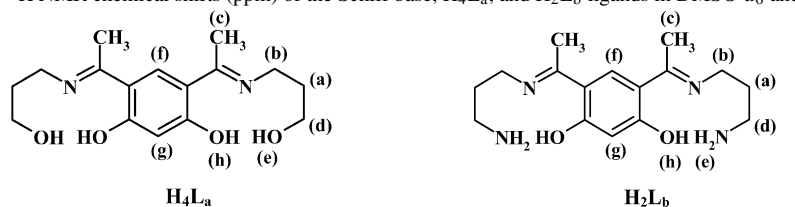
Fig. 1. ^1H NMR spectra (δ , ppm) in $\text{DMSO}-d_6$ solvent of the (a) Schiff base, H_4L_a , ligand, (b) expansion of the range 5.5–8.5 ppm from the spectrum (a), (c) Schiff base, H_4L_a , ligand after the addition of D_2O , (d) Schiff base, H_2L_b , ligand, (e) expansion of the range 1.0–3.4 ppm from the spectrum (d) and (f) Schiff base, H_2L_b , ligand after the addition of the D_2O ; * suppressed solvent.

complexes are listed in Table 4. The assignments were aided by comparison with the vibrational frequencies of the free ligands and their related compounds [20].

There are four conceptual features in the infrared spectra of the complexes. The first feature is the shift of the stretching frequencies of azomethine $\nu(-\text{C}=\text{N}-)$ group of the metal complexes which are in lower frequencies and lie in the range of $1538\text{--}1559\text{ cm}^{-1}$, for the former ligand complexes, and $1530\text{--}1575$ for the later ligand complexes compared with the free H_4L_a and H_2L_b ligand bands at 1578 and 1575 cm^{-1} , respectively, which may be due to the coordination of the two azomethine groups to metal ions [21,22]. In the case of $\text{Cu}(\text{II})$ complex (8) and $\text{Ni}(\text{II})$ complex (9), it was found that, the value

of $\nu(-\text{C}=\text{N}-)$ did not change compared to the free H_2L_b ligand. This may be due to the interference of the deformation vibration of H_2O molecules, $\delta(\text{H}_2\text{O})$, with the stretching vibration of the azomethine group, $\nu(-\text{C}=\text{N}-)$ [19]. The second feature is the broad bands in the range of $3333\text{--}3445\text{ cm}^{-1}$ which can be assigned to the stretching frequencies of the $\nu(\text{OH})$ of methanol, OH-phenolic and/or the water molecules associated to the complexes which are also confirmed by the elemental analyses. The third feature is the weak bands at $(419\text{--}522\text{ cm}^{-1})$ and $(561\text{--}615\text{ cm}^{-1})$, ranges which could be assigned to the stretching frequencies of the $\nu(\text{M}-\text{O})$ and $\nu(\text{M}-\text{N})$ bands for the transition metal complexes of both H_4L_a and H_2L_b ligands, respectively [23], supporting that the bonding of the ligand

Table 3
¹H NMR chemical shifts (ppm) of the Schiff base, H₄L_a, and H₂L_b ligands in DMSO-*d*₆ and their assignments

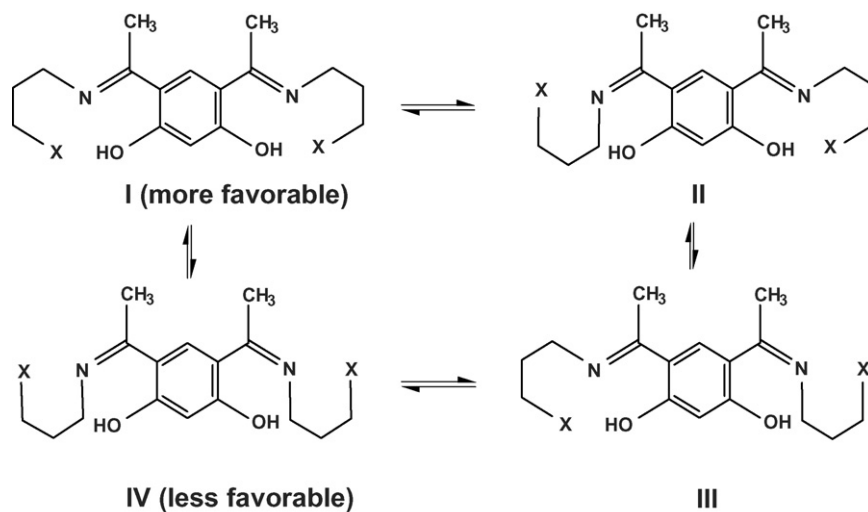


Chemical shifts (ppm)		Assignments
H ₄ L _a	H ₂ L _b	
1.59	1.58	[m, 4H, 2CH ₂] (a)
1.79	1.80	[t, 4H, 2CH ₂] (b)
2.41	2.41	[s, 6H, 2CH ₃] (c)
2.69	2.67	[t, 4H, 2CH ₂] (d)
4.62*	3.31*	[s, br, 2H, 2OH] (e) or [s, br, 4H, 2NH ₂] (e)
5.86 and 8.17	(5.44, 5.70 and 5.80 centered at 5.65) and (7.78, 8.03 and 8.18 centered at 8.00)	[s, 1H, Ar-H] (f) and [s, 1H, Ar-H] (g)
17.28*	17.28*	[s, 2H, 2OH] (h)

(1) s: singlet, t: triplet, br: broad, m: multiplet. (2) Data given from the spectra depicted in Fig. 1. (3) Chemical shifts (ppm) were referenced internally at 25 °C with respect to TMS. (4) Asterisks (*) denote the bands disappeared after the addition of D₂O.

to the metal ions is achieved by the alcoholic and/or phenolic oxygen atoms, the azomethine and amino nitrogen atoms of the ligands. The fourth feature is the coordination behavior of nitrate and sulfate anions. The NO₃⁻ ions are coordinated to the metal center as unidentate ligands for the complexes (1), (2), (3) and (4) with C_{2v} symmetry. Each unidentate nitrate group possesses three non-degenerated modes of the vibrations (ν_s , ν_{as} and ν_{as}), which appeared at the ranges 1381–1434, 1317–1356 and 802–810 cm⁻¹, respectively, for the metal complexes which contain the nitrate groups, the middle band is further splits in the case of Co(II) and Cr(III) complexes [23]. The ν_s (NO₃⁻) of the unidentate NO₃⁻ is markedly shifted to lower frequencies compared to that of the free nitrate (1700–1800 cm⁻¹) [23]. This could be a factor measuring the covalent bond strength which is formed due to the transfer of an electron density from NO₃⁻ to

the metal ion. In complex (5), two NO₃⁻ ions behave as bidentate ligand. These nitrate groups possess three non-degenerated modes of the vibrations (ν , ν_a and ν_s), which appeared at 1542, 1325, and 811 cm⁻¹. Beside, there are two ionic NO₃⁻ groups in the Cr(III) complex, their vibrations appeared at 1354 and 1054 cm⁻¹. The SO₄²⁻ anion is also coordinated as bridging bidentate ligand in the [(VO)₂(L_b)(SO₄)(H₂O)₂].2H₂O complex (13). Generally, the free sulfate ion belongs to the high-symmetry point group T_d [23]. Of the four fundamentals, only ν_3 and ν_4 are infrared active. If the symmetry of the SO₄²⁻ anion is lowered by complex formation, the degenerate vibrations split and also ν_1 and ν_2 appear in the infrared spectrum [23]. In case of [(VO)₂(L_b)(SO₄)(H₂O)₂].2H₂O complex (13), also ν_1 and ν_2 appear with medium intensity at 1056 and 455 cm⁻¹, respectively, moreover, ν_3 and ν_4 each splits, where ν_3 splits into 1124



H₄L_a for X = OH and H₂L_b for X = NH₂

Scheme 3. Tautomeric structures of the Schiff base, H₄L_a and H₂L_b ligands.

Table 4
Characteristic infrared frequencies (cm^{-1})^a of the Schiff base, H₄L_a and H₂L_b ligands and their transition metal complexes

Ligand/complex	$\nu(\text{OH})$		$\nu_{\text{as}}(\text{NH}_2)$	$\nu_{\text{s}}(\text{NH}_2)$	$\delta(\text{H}_2\text{O})$	$\nu(\text{C}=\text{C})$	$\nu(\text{C}=\text{N})$	$\nu(\text{M}-\text{N})$	$\nu(\text{M}-\text{O})$	Other bands
	H ₂ O and/or CH ₃ OH	Phenolic and/or alcoholic								
H ₄ L _a	–	3215 s, br	–	–	–	1615 vs, br	1578 vs, br	–	–	–
H ₂ L _b		3422 s, br	3250 s, sh	–	1625 vs, sh	1575 vs, br	–	–	–	–
(1) Cu ₂ (H ₂ L _a)(NO ₃) ₂ ·2CH ₃ OH	3412 s, br	3225 s, br	–	–	–	1596 vs, br	1543 vs, br	615 m	504 w	1404 s, 1326 s, 805 w, unidentate NO ₃ groups
(2) [Ni ₂ (H ₂ L _a)(NO ₃) ₂ (CH ₃ OH) ₂ (H ₂ O) ₂]	3333 s, br	3255 s, sh	–	–	–	1583 vs, br	1559 vs, br	602 m	522 w	1413 s, 1326 s, 804 w, unidentate NO ₃ groups
(3) [Co ₂ (H ₂ L _a)(H ₂ O) ₂ (CH ₃ OH) ₂ (NO ₃) ₂]	3389 s, br	3242 s, br	–	–	–	1562 vs, br	1557 vs, br	590 m	500 w	1417 s, 1323s, 802 w, unidentate NO ₃ groups
(4) [Fe ₂ (L _a)(H ₂ O) ₄ (NO ₃) ₂ ·2H ₂ O	3390 s, br	3250 s, br	–	–	–	1597 vs, br	1538 vs, br	602 m	513 w	1382 s, 1317 s, 807 w, unidentate NO ₃ groups
(5) [Cr ₂ (H ₂ L _a)(H ₂ O) ₂ (NO ₃) ₂](NO ₃) ₂ ·2H ₂ O·3CH ₃ OH	3404 s, br	3233 s, br	–	–	–	1601 vs, br	1542 vs, br	613 m	510 m	1542 vs, 1325 sh, 811 w, bidentate NO ₃ groups
(6) [(VO) ₂ (L _a)(H ₂ O) ₂ ·2H ₂ O	3442 m, br	3233 m, br	–	–	–	1594 vs, br	1540 vs, br	613 w	502 w	986 w, $\nu(\text{V}=\text{O})$
(7) [(UO ₂) ₂ (H ₂ L _a) ₂ ·6H ₂ O	3421 m, br	3250 m, br	–	–	–	1555 vs, br	593 w	–	487 w	905 s, $\nu(\text{UO}_2)$
(8) [Cu ₂ (L _b)(NO ₃) ₂ (H ₂ O) ₄ ·H ₂ O	3423 s, br		3250 s, sh	–	–	1575 s, br		596 w	510 w	1421 s, 1321 s, 808 w; unidentate NO ₃ groups
(9) [Ni ₂ (L _b)(NO ₃) ₂ (H ₂ O) ₄ ·2CH ₃ OH	3418 s, br		3250 s, sh	–	1577 vs, br	1577 vs, br		601 w	496 w	1434 m, 1329 s, 810 w, sh; unidentate NO ₃ groups
(10) [Co ₂ (L _b)(NO ₃) ₂ (H ₂ O) ₄ ·3H ₂ O	3422 vs, br		3250 s, sh	3146 s, sh	1577 vs, br	1546 vs		598 w	519 w	1426 m, 1352 vs, 1297 m, sh, 810 w, sh; unidentate NO ₃ groups
(11) [Cd ₂ (L _b)(NO ₃) ₂ (H ₂ O) ₄ ·3H ₂ O	3445 s, br		3250 s, sh	–	1578 vs, br	1556 s, sh		580 w	492 vw	1420 s, sh, 1311 s, br, 810 w, sh; unidentate NO ₃ groups
(12) [Cr ₂ (L _b)(NO ₃) ₄ (H ₂ O) ₂ ·4.5H ₂ O	3415 s, br		3250 m, sh	–	1599 s, br	1540 s, br		561 m	484 m	1381 vs, 1356 s, 1297 s, 810 w, sh; unidentate NO ₃ groups
(13) [(VO) ₂ (L _b)(SO ₄)(H ₂ O) ₂ ·2H ₂ O	3419 s, br		3208 s, sh	3144 s, sh	1580 vs, sh	1564 vs		600 sh	500 w, sh	1124 s, 1095 s, sh, 1056 s, sh, 625 m, 612 m, 455 w, sh; bridging SO ₄ groups, 942 m, sh; $\nu(\text{V}=\text{O})$
(14) [(UO ₂) ₂ (L _b) ₂ (H ₂ O) ₄ ·4H ₂ O	3420 m, br		3250 s, sh	–	1578 vs	1530 s, sh		587 vw	419 vw	897 m; $\nu_3(\text{UO}_2)$

^a s: strong, m: medium, w: weak, v: very, vs: very strong, sh: shoulder, and br: broad.

Table 5
Characteristic electronic spectral bands (nm) and magnetic moments of the Schiff base, H₄L_a and H₂L_b ligands and their transition metal complexes

Ligand/complex	λ_{\max} (nm) ^a	Assignments	Magnetic moments (μ_B)	
			$\mu_{\text{compl.}}^b$	$\mu_{\text{eff.}}^c$
(1) [Cu ₂ (H ₂ L _a)(NO ₃) ₂].2CH ₃ OH	675	$^3T_{2g}(G) \leftarrow E_g$	2.43	1.72
(2) [Ni ₂ (H ₂ L _a)(NO ₃) ₂ (CH ₃ OH) ₂ (H ₂ O) ₂]	480, 693, 1080	$^3T_{1g}(P) \leftarrow ^3A_{2g}(F)$, $^3T_{1g}(F) \leftarrow ^3A_{2g}(F)$, $^3T_{2g}(F) \leftarrow ^3A_{2g}(F)$	4.89	3.11
(3) [Co ₂ (H ₂ L _a)(H ₂ O) ₂ (CH ₃ OH) ₂ (NO ₃) ₂]	605	$^4A_{2g}(F) \leftarrow ^4T_{1g}(F)$	5.85	4.81
(4) [Fe ₂ (L _a)(H ₂ O) ₄ (NO ₃) ₂].2H ₂ O	500, 533, 691	Charge transfer tailing from UV to visible region	6.70	4.74
(5) [Cr ₂ (H ₂ L _a)(H ₂ O) ₂ (NO ₃) ₂](NO ₃) ₂ .2H ₂ O.3CH ₃ OH	485 605	$^4T_{1g}(F) \leftarrow ^4A_{2g}(F)$ $^4T_{2g}(F) \leftarrow ^4A_{2g}(F)$	5.47	3.87
(6) [(VO) ₂ (L _a)(H ₂ O) ₂].2H ₂ O	652	b ₁ \leftarrow b ₂	1.70	1.20
(7) [(UO ₂) ₂ (H ₂ L _a) ₂].6H ₂ O	509	Charge transfer	–	–
(8) [Cu ₂ (L _b)(NO ₃) ₂ (H ₂ O) ₄].H ₂ O	668	$^3T_{2g}(G) \leftarrow E_g$	3.07	2.17
(9) [Ni ₂ (L _b)(NO ₃) ₂ (H ₂ O) ₄].2CH ₃ OH	444, 526	$^3T_{1g}(P) \leftarrow ^3A_{2g}(F)$, $^3T_{1g}(F) \leftarrow ^3A_{2g}(F)$	4.39	3.10
(10) [Co ₂ (L _b)(NO ₃) ₂ (H ₂ O) ₄].3H ₂ O	631	$^4A_{2g}(F) \leftarrow ^4T_{1g}(F)$	7.19	5.08
(11) [Cd ₂ (L _b)(NO ₃) ₂ (H ₂ O) ₄].3H ₂ O	–	–	–	–
(12) [Cr ₂ (L _b)(NO ₃) ₄ (H ₂ O) ₂].4.5H ₂ O	615, 745	$^4T_{1g}(F) \leftarrow ^4A_{2g}(F)$, $^4T_{2g}(F) \leftarrow ^4A_{2g}(F)$	5.38	3.81
(13) [VO] ₂ (L _b)(SO ₄)(H ₂ O) ₂].2H ₂ O	674	b ₁ \leftarrow b ₂	–	–
(14) [(UO ₂) ₂ (L _b) ₂ (H ₂ O) ₄].4H ₂ O	485	Charge transfer	–	–

^a Reflectance spectra of all complexes were recorded with disks made by compressing a mixture of the complex sample with suitable amount of NaCl (Analar). Also, NaCl compressed disk was used as a reference sample.

^b $\mu_{\text{compl.}}$ is the magnetic moment of all metal ions present in the complex.

^c $\mu_{\text{eff.}}$ is the magnetic moment of one metal ion in the complex.

and 1095 cm⁻¹, and ν_4 splits into 625 and 612 cm⁻¹. These splitting can be explained by a lowering of symmetry, where the bridging bidentate sulfato group belongs to C_{2v} point group [23].

The IR spectra of VO(IV) complexes display a band at 986 cm⁻¹ for complex (6) and a shoulder band at 942 cm⁻¹ for complex (13) which have no counterpart in the spectrum of the H₄L_a and H₂L_b ligands and are assigned to the stretching frequency of the $\nu(V=O)$. Also, The IR spectra of the UO₂(VI) complexes display a characteristic band for complexes (7) and (14) at 905 and 897 cm⁻¹, respectively, which are assigned to the stretching frequency of the $\nu(UO_2)$.

3.2.2. Electronic, mass and ESR spectra and magnetic moment measurements

The metal complexes are insoluble in most common solvents and were not possible to get electronic spectra in solution. The electronic spectra were obtained by reflectance within the range 400–1200 nm. It is possible to draw up the electronic transitions and predict the geometry with the aid of magnetic moments of most metal ions. Table 5 lists the electronic spectral bands and the magnetic moments of the metal ions in their complexes in the solid state.

The electronic spectrum of the green Cu(II) complexes (1) and (8) showed one band due to $^3T_{2g}(G) \leftarrow E_g$ transition, which was observed at 675 and 668 nm, respectively. The measured value of the magnetic moment for Cu(II) complex was 1.72 μ_B , for the former complex (1) and 2.17 μ_B for the later complex (8), which confirms the square planar structure for

complex (1) and octahedral structure for complex (8) [24]. X-Band ESR spectra of [Cu₂(H₂L_a)(NO₃)₂].2CH₃OH (1) and [Cu₂(L_b)(NO₃)₂(H₂O)₄].H₂O (8), Fig. 2a and b, were recorded in the solid state at 25 °C. The spectrum of the former complex exhibits one broad band with $g = 2.1081$. The shape of the spectrum is consistent with the square planar geometry around each Cu(II) ion in the complex [24,25]. The spectrum for complex (8) exhibits two bands, one of them is sharp with $g = 2.1003$ and the other is very weak at $g = 2.0023$. The shape of the spectrum is consistent with the octahedral geometry around each Cu(II) center in the complex.

The electronic spectrum of the green Ni(II) complexes (2) and (9) showed several bands. Generally, three spin-allowed transitions are expected, because of the splitting of the free-ion, ground 3F term and the presence of the 3P -term [25–27]. Usually, the spectra of octahedral Ni(II) consist of three bands which are accordingly assigned as $^3T_{2g}(F) \leftarrow ^3A_{2g}(F)$, $^3T_{1g}(F) \leftarrow ^3A_{2g}(F)$ and $^3T_{1g}(P) \leftarrow ^3A_{2g}(F)$. The $^3T_{2g}(F) \leftarrow ^3A_{2g}(F)$ transition was observed at 1080 nm, in complex (2) and was not observed in complex (9), as it occurs in the near infrared and thus out of the instrument. The $^3T_{1g}(F) \leftarrow ^3A_{2g}(F)$ transition was observed at 693 nm and 526 nm, for both complex (2) and complex (9), respectively. The third band due to $^3T_{1g}(P) \leftarrow ^3A_{2g}(F)$ transition was observed at 480 nm for the former complex, while in the second complex this transition is obscured by ligand absorption bands. The magnetic moments were measured which gave 3.11 and 3.10 μ_B , for complexes (2) and (9), respectively, which lies in the range (2.9–3.3 μ_B) of the Ni(II) octahedral complexes [23]. The mass spectrum of the, [Ni₂(L_b)(NO₃)₂(H₂O)₄].2CH₃OH, complex (9) showed the parent peak at m/e 617 which compares

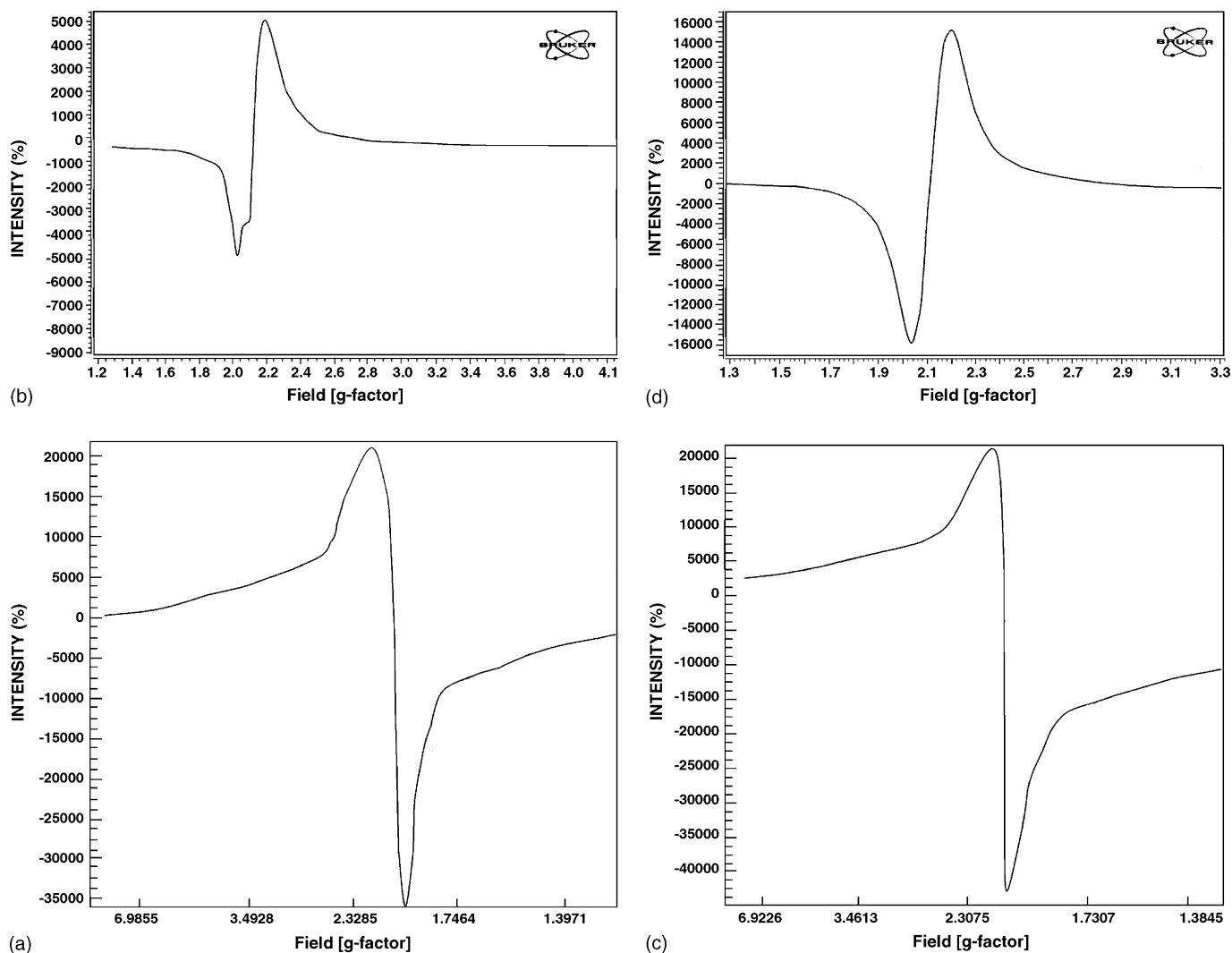


Fig. 2. X-Band ESR spectra of: (a) $[\text{Cu}_2(\text{H}_2\text{L}_a)(\text{NO}_3)_2] \cdot 2\text{CH}_3\text{OH}$ (**1**), (b) $[\text{Cu}_2(\text{L}_b)(\text{NO}_3)_2(\text{H}_2\text{O})_4] \cdot \text{H}_2\text{O}$ (**8**), (c) $[(\text{VO})_2(\text{L}_a)(\text{H}_2\text{O})_2] \cdot 2\text{H}_2\text{O}$ (**6**) and (d) $[(\text{VO})_2(\text{L}_b)(\text{H}_2\text{O})_2] \cdot 2\text{H}_2\text{O}$ (**13**) complexes.

well with the formula weight of the complex after loss of the two uncoordinated methanol molecules.

The electronic spectra of the green Co(II) complexes ((**3**) and (**10**)) showed that, both complexes have an octahedral geometry. The transitions can be interpreted by using Tanabe-Sugano diagram. In the Co(II) octahedral complexes the spectra usually consist of three bands [25]. The first band, which is due to ${}^4\text{T}_{2g}(\text{F}) \leftarrow {}^4\text{T}_{1g}(\text{F})$ transition, this band was not observed due to the fact that it occurs in the near infrared region, and out of the range of the used instrument. The other two bands were observed in the visible region, the former one is due to ${}^4\text{A}_{2g}(\text{F}) \leftarrow {}^4\text{T}_{1g}(\text{F})$ transition, which is observed at 605 and 631 nm for complexes ((**3**) and (**10**)), respectively. The second band due to ${}^4\text{T}_{1g}(\text{P}) \leftarrow {}^4\text{T}_{1g}(\text{F})$ transition is expected at 450 nm was not distinguished as it may be overlapped by charge transfer band or it would be obscured by ligand transition. The Co(II) complex showed the magnetic moment 4.81 and $5.08\mu_{\text{B}}$ for complexes (**3**) and (**10**), respectively, at room temperature where that of the usual octahedral complexes are 4.8–5.2 B.M [26]. The mass spectrum of the Co(II) complex, $[\text{Co}_2(\text{L}_b)(\text{NO}_3)_2(\text{H}_2\text{O})_4] \cdot 3\text{H}_2\text{O}$

(**10**), showed the molecular ion peak at m/e 672 which agrees well with the formula weight of the complex (FW 672.4).

The electronic spectrum of the red Fe(III) complex (**4**) showed strong bands at 500, 533 nm and a weak band at 961 nm. It was not possible to identify the type of the d–d transition. This is due to a strong charge transfer (CT) band tailing from the UV-region to the visible region. Generally, from the elemental and the infrared spectrum which gives a significant proof for the nitrate anion to act as a unidentate ligand, it is expected that the Fe(III) complex has octahedral arrangement. Magnetic moment of the Fe(III) complex was measured and gives $4.74\mu_{\text{B}}$. This value is lower than the magnetic moment of the high spin octahedral, $t_{2g}^3 e_g^2$ arrangement, which amounts to 5.92 B.M [27]. A complete interpretation of the lower value than normal was not possible without knowing the crystal structure of the complex. On the other hand, the experimental value is too far higher than the low spin octahedral, $(t_{2g}^5 e_g^0)$ arrangement, where its magnetic moment amounts to 2.3 B.M [26]. Generally, a tentative interpretation expects the structure of Fe(III) as high-spin octahedral geometry, with antiferromagnetic interaction.

The Cd(II) complex (**11**) is diamagnetic as expected and its geometry is most probably octahedral similar to the Cu(II), Ni(II) and Co(II) complexes of the H_2L_b ligand.

The electronic spectrum of the dark green Cr(III) complexes (**5**) and (**12**) showed an octahedral geometry. In the Cr(III) octahedral complexes, the splitting of the free ion ground F term along with the presence of the excited P-term of the same multiplicity provides the possibility of three spin allowed d–d transitions [28]. The first two bands which are due to ${}^4T_{2g}(F) \leftarrow {}^4A_{2g}(F)$ and ${}^4T_{1g}(F) \leftarrow {}^4A_{2g}(F)$ transitions, were observed at 605 and 485 nm, for the complex (**5**) and 745 and 615 nm, for the complex (**12**). The third band which is due to ${}^4T_{1g}(P) \leftarrow {}^4A_{2g}(F)$ transition lies in the range of the ligand transitions and is not possible to be identified. The magnetic moment is expected to be very close to the spin-only value for three unpaired electrons, due to the absence of any orbital contribution. In the present work, the magnetic moments of the Cr(III) complexes (**5**) and (**12**) are 3.87 and 3.81 B.M, respectively.

The electronic spectrum of the green VO(IV) complexes (**6**) and (**13**) showed one band at 652 and 674 nm, respectively, which corresponds to $b_1 \leftarrow b_2$ electronic transition [27]. With the aid of the elemental analysis and the infrared spectra, the VO(IV) complexes (**6**) is 5-coordinate which would be square pyramidal and the complex (**13**) is 6-coordinate

which would be octahedral structure. Although most oxovanadium(IV) complexes are magnetically simple which having virtually 'spin-only' moments of $1.73\mu_B$ corresponding to one unpaired electron. In this study, the actual magnetic moments were 1.20 and $1.22\mu_B$ for complexes (**6**) and (**13**), respectively. These values are less than the expected and could be due to antiferromagnetic effect between vanadium atoms of adjacent molecules linked together through oxygen atoms.

The X-band ESR spectra of VO(IV) complexes (**6**) and (**13**), Fig. 2c and d, were recorded in the solid state at 25°C . The ESR spectra of the oxovanadium, $[\text{VO}_2\text{-sq. py.}]$, (**6**), and $[\text{VO}_2\text{-oct.}]$ (**13**) complexes, exhibit one broad band centered on $g = 2.1081$ and $g = 2.1085$, respectively, without resolved hyperfine structure. In particular, the hyperfine coupling with nearly ${}^{51}\text{V}$ ($I = 7/2, S = 1/2$) nucleus is not observable. The absence of vanadium's hyperfine coupling is common in the solid state [29] and is attributed to the simultaneous flipping of neighboring electron spin [30] or due to strong exchange interactions, which average out the interaction with the nuclei. For $[\text{VO}_2\text{-sq. py.}]$, upon pairing the two vanadium ions, the two electron spins may combined to give a non-magnetic spin singlet ($S = 0$) or a paramagnetic spin triplet ($S = 1$). Only the latter ESR is detectable $\Delta_{\text{ms} \pm 2}$ [31]. In the present complex, there is a slight interaction between the two magnetically vanadium centers which is consistent with

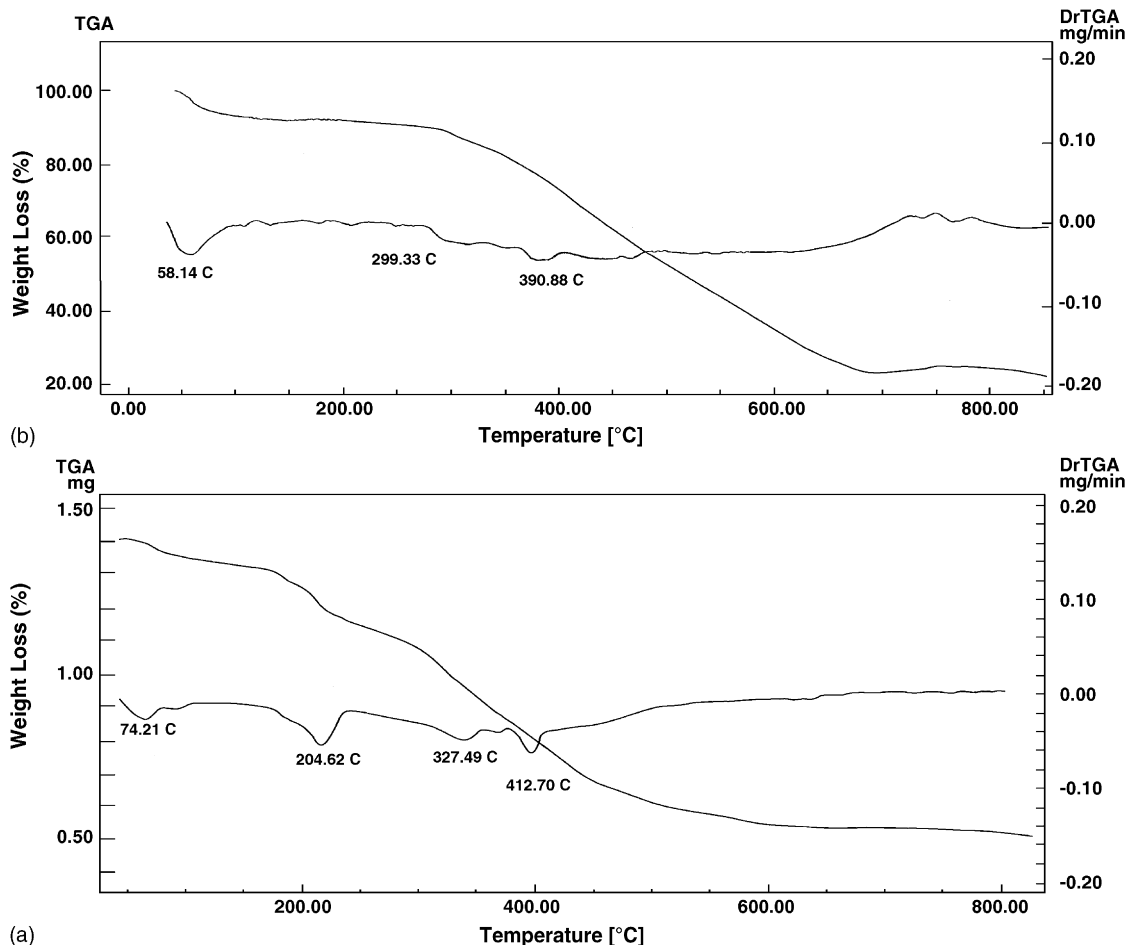


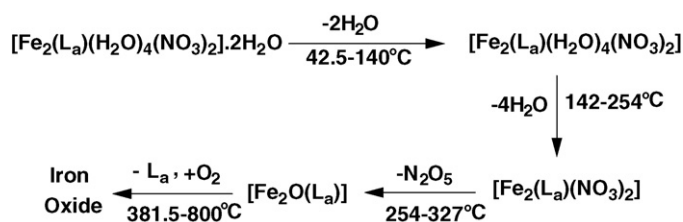
Fig. 3. TGA–DrTGA curves of: (a) $[\text{Fe}_2(\text{HL}_a)(\text{H}_2\text{O})_4(\text{NO}_3)_2] \cdot 2\text{H}_2\text{O}$ (**4**) and (b) $[\text{Ni}_2(\text{L}_b)(\text{NO}_3)_2(\text{H}_2\text{O})_4] \cdot 2\text{CH}_3\text{OH}$ (**9**) complexes.

normal-effective magnetic moment. Square-pyramid geometry is proposed for the binuclear complexes. The value of the magnetic moment ($1.20\mu_B$) agrees well with the proposed structures. For ($\text{VO}_2\text{-oct.}$) complex the shape of the spectrum as well as the spectral studies agree with the proposed structures.

The electronic spectrum of the yellow $\text{UO}_2(\text{VI})$ complexes (7) and (14) arises from the electronic transition of metal \rightarrow ligand charge transfer. This is an allowed transition and produces a broad, intense absorption band at 509 and 485 nm for complexes (7) and (14), respectively, tailing into the visible region. This produces the intense yellow color, where the $\text{UO}_2(\text{VI})$ complexes are diamagnetic as expected [32].

3.2.3. Thermal gravimetric analysis

Thermal gravimetric analysis (TGA) was used as a probe to proof the associated water or solvent molecules to be in the coordination sphere or in the crystalline form [33]. TGA curve of $[\text{Fe}_2(\text{L}_a)(\text{H}_2\text{O})_4(\text{NO}_3)_2]\cdot 2\text{H}_2\text{O}$, complex (4), shows four stages, Scheme 4. The former one is at $42.5\text{--}140^\circ\text{C}$ with the loss of two hydrated water molecules (Calc./Found%; 5.55/ 6.18%) of the total weight of the complex. The second stage at $142\text{--}254^\circ\text{C}$ corresponds to the loss of four coordinated water molecules (Calc./Found%; 11.76/13.91%). The third stage at $254\text{--}381.5^\circ\text{C}$ corresponds to the loss of N_2O_5 gas molecules (Calc./Found%; 20.00/ 21.34%). The later stage was at $381.5\text{--}800^\circ\text{C}$ and is due to the gradual decomposition of the complex. The residue was 37.63% of the total weight which may be ascribed to the formation of iron(III) oxide. The first two stages are the important stages to identify the coordinated and crystalline water



Scheme 4. Thermal degradation pattern of Fe(III) complex, $[\text{Fe}_2(\text{L}_a)(\text{H}_2\text{O})_4(\text{NO}_3)_2]\cdot 2\text{H}_2\text{O}$ (4).

molecules in complex (4). DrTGA curve of the complex exhibits two endothermic peaks. The first peak was at 74°C which is ascribed to the loss of crystalline water molecules while the second peak at 204°C is due to the loss of coordinated water molecules. Also, there are two exothermic peaks, the first one was at 381.5°C which is due to the loss of N_2O_5 molecules and the second peak was at 440°C which is due to the decomposition and phase transfer of the complex. Fig. 3a shows the TGA–DrTGA curves of the $[\text{Fe}_2(\text{L}_a)(\text{H}_2\text{O})_4(\text{NO}_3)_2]\cdot 2\text{H}_2\text{O}$ (4) complex.

Thermal gravimetric analysis (TGA) for complex (9), $[\text{Ni}_2(\text{L}_b)(\text{NO}_3)_2\text{--}(\text{H}_2\text{O})_4]\cdot 2\text{CH}_3\text{OH}$, shows two stages in the range $30\text{--}310^\circ\text{C}$. The former one at $35\text{--}120^\circ\text{C}$, is due to the loss of two uncoordinated methanol molecules (weight loss; Calc./Found%; 9.4/9.1%). The second stage at $140\text{--}310^\circ\text{C}$ and is due to the loss of four coordinated water molecules (weight loss; Calc./Found%; 10.5/10.4%). Fig. 3b shows the TGA–DrTGA curves of complex (9).

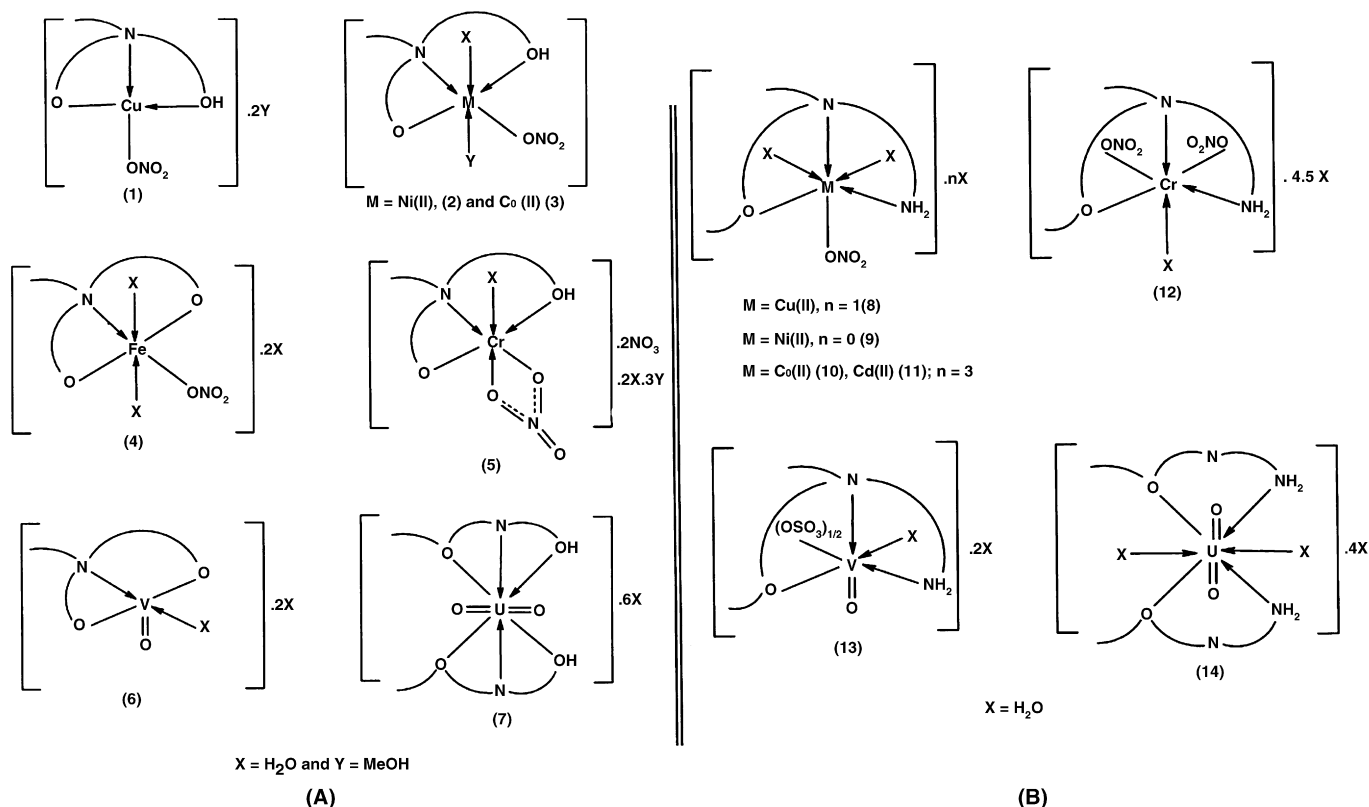


Fig. 4. Representative structures of the transition metal complexes of the Schiff base (A) H_4L_a ligand and (B) H_2L_b ligand.



Scheme 5. Thermal degradation pattern of complex (9) in the range of 30–310 °C.

Scheme 5 is the thermal degradation pattern of complex (9), $[\text{Ni}_2(\text{L}_b)(\text{NO}_3)_2(\text{H}_2\text{O})_4] \cdot 2\text{CH}_3\text{OH}$, in the range of 30–310 °C.

Finally, from the interpretation of elemental analysis and infrared, mass, electronic spectra, ESR for Cu(II) and VO(IV) complexes and TGA for Ni(II) complex, it is possible to draw up the tentative structures of the transition metal complexes. Fig. 4 depicts the proposed structures of the metal complexes.

References

- [1] S. Park, V.K. Mathur, R.P. Planap, *Polyhedron* 17 (1998) 325.
- [2] A. Nashinaga, H. Ohara, H. Tomita, T. Matsuura, *Tetrahedron Lett.* 24 (1983) 213.
- [3] L.F. Lindoy (Ed.), *The Chemistry of Macrocyclic Ligand Complexes*, Cambridge University Press, Cambridge, 1989.
- [4] K. Maruyama, K. Kubo, Y. Toda, K. Kawasa, T. Mashino, A. Nishinaga, *Tetrahedron Lett.* 36 (1995) 5609.
- [5] T. Nakamura, K. Niwa, M. Fujiwara, T. Matsushita, *Chem. Lett.* 1067 (1999).
- [6] Y.K. Choi, W.S. Kim, K.I. Chung, M.W. Chung, H.P. Nam, *Microchem. J.* 65 (2000) 3.
- [7] C.J. Burrows, J.G. Muller, G.T. Poulter, S.E. Rokita, *Acta Chem. Scand.* 50 (1996) 337.
- [8] H. Yoon, T.R. Wagler, K.J. O'Connor, C.J. Burrows, *J. Am. Chem. Soc.* 122 (1990) 4568.
- [9] M.A. Green, H. Luo, P.E. Fanwick, *Inorg. Chem.* 37 (1998) 1127.
- [10] A.A.A. Emara, A.A.A. Abou-Hussen, *Spectrochim. Acta (A)* 64 (2006) 1010.
- [11] H.S. Seleem, A.A.A. Emara, M. Shebl, *J. Coord. Chem.* 58 (2005) 1003.
- [12] H.A. Flaschka, *EDTA Titration*, 2nd ed., Pergamon Press, 1964, p. 81.
- [13] A.I. Vogel, *Textbook of Quantitative Inorganic Analysis*, 4th ed., Longman, London, 1978.
- [14] T.S. West, *Complexometry with EDTA and Related Reagents*, 3rd ed., DBH Ltd., Pools, 1969.
- [15] F.E. Mabbs, D.I. Machin, *Magnetism and Transition Metal Complexes*, Chapman and Hall, London, 1973.
- [16] E.C. Alyea, A. Malek, *Can. J. Chem.* 53 (1975) 939.
- [17] R.J. Platt, *J. Chem. Phys.* 17 (1949) 484.
- [18] E. Pretsch, J. Seibl, *Tables of Spectral Data for Structure Determination of Organic Compounds*, Springer-Verlag, Berlin, 1983.
- [19] A.A.A. Abou-Hussen, A.A.A. Emara, *J. Coord. Chem.* 57 (2004) 973.
- [20] B. Jazowska, J. Lisowshi, A. Vogt, P. Chemielewski, *Polyhedron* 7 (1988) 337.
- [21] S.M.E. Khalil, A.A.A. Emara, *J. Coord. Chem.* 55 (2002) 17.
- [22] B.A. El-Sayed, M.M. Abo Aly, A.A.A. Emara, S.M.E. Khalil, *Vibr. Spectrosc.* 93 (2002) 30.
- [23] K. Nakamoto, *Infrared Spectra of Inorganic and Coordination Compounds*, 5th ed., John Wiley and Sons, New York, 1997.
- [24] A.A.A. Emara, *Synth. React. Inorg. Met. -Org. Chem.* 29 (1999) 87.
- [25] N.N. Greenwood, A. Earnshaw, *Chemistry of the Elements*, Pergamon Press, New York, 1984.
- [26] F.A. Cotton, G. Wilkinson, *Advanced Inorganic Chemistry. A Comprehensive Text*, 4th ed., John Wiley and Sons, New York, 1986.
- [27] J.C. Bailar, H.J. Emeleus, R. Nyholm, A.F. Trotman-Dickenson, *Comprehensive Inorganic Chemistry*, vol. 3, Pergamon Press, 1975.
- [28] A.B.P. Lever, *Inorganic Electronic Spectroscopy*, 2nd ed., Elsevier, New York, 1997.
- [29] A.A. Abou-Hussen, N.M. El-Metwally, E.M. Soad, A.A. El-Asmy, *J. Coord. Chem.* 58 (2005) 1735.
- [30] A. Bencini, D. Gatteschi, *EPR of Exchange Coupled Systems*, Springer, Verlach, Berlin, 1990.
- [31] N.M. El-Metwally, I.M. Gaber, A.A. El-Asmy, A.A. Abou-Hussen, *Trans. Met. Chem.* 31 (2006) 71.
- [32] E. Rabinowitch, R.L. Belford, *Spectroscopy and Photochemistry of Uranyl Compounds*, Pergamon Press, New York, 1984.
- [33] A.A.A. Emara, F.S.M. Abd El-Hameed, S.M.E. Khalil, *Phosphor. Sulfur Silicon* 114 (1996) 1.